BARIUM TITANATE THIN FILMS FOR NOVEL MEMORY APPLICATIONS

Laura STOICA[1], Faye BYGRAVE[2], Andrew J. BELL[3]

Within this work, $BaNb_xTi_{(1-x)}O_3/BaTiO_3$, with x=0.01 and 0.02 thin films have been epitaxially deposited by Pulsed Laser Deposition (PLD) on $SrRuO_3/SrTiO_3$, where $SrRuO_3$ represents the bottom electrode deposited on single crystal substrate $SrTiO_3$. At the interface, the films are expected to show the Positive Temperature Coefficient Resistor (PTCR) effect, which is a possible novel mechanism for memory applications. The phase, structure and lattice parameters have been investigated by X-ray Diffraction (XRD). Scanning Electron Microscopy (SEM) and Atomic Force Microscopy (AFM) have been used to analyse the thickness and topography, whilst Piezoresponse Force Microscopy (PFM) has been used to visualise the ferroelectric domains.

Keywords: barium titanate, thin films, oxide heterostructures, PTCR.

1. Introduction

The amount of stored information in the wide world doubles every three years. This represents a motivation to improve the existent memory devices, but also to develop new mechanisms of storing information. Currently, the market is dominated by Hard Disk Drives (HDD) and also Flash memories. HDDs have the advantage of being cheap with a high capacity. However they are slow and if shocked, they may fail and data may be lost. In addition, Flash memories are faster, but relatively costly. Therefore, there is a growing need of developing a new type of memory device – with large storage density, cheap, fast, with low power consumption and high endurance [1]. Since the discovery of first ferroelectric ceramic material – $BaTiO_3$ (BT) it was suggested that this may offer the possibility of a two state device, electrically switchable [2]. Since then, ferroelectric memories have been developed and they already found their place on the market within smart debit card or Play Station 2 [3]. This type of memories, are based on the following principle: ferroelectric materials exhibit a net polarisation (the sum of all dipoles in the material) which can be reversed by application of an electric field. A memory cell is represented by two components:

[1] Institute for Materials Research, University of Leeds, Leeds, LS2 9JT, UK, e-mail: sm11las@leeds.ac.uk
[2] Institute for Materials Research, University of Leeds, Leeds, LS2 9JT, UK
[3] Institute for Materials Research, University of Leeds, Leeds, LS2 9JT, UK

a capacitor made by the ferroelectric material and a transistor used to switch the polarisation [4]. However, in this work, another phenomenon shall be exploited, namely the positive temperature coefficient resistor (PTCR), which represents a change in the resistance of the material, by several orders of magnitude, with increasing the temperature. This effect is exhibited by donor doped ceramics. Owing to the fact that PTCR is not observed in the single crystal form, it is assumed that the change in resistance is associated with grain boundaries [5]. Therefore, the question arises if this phenomenon occurs at the interfaces of epitaxial thin film layers in a heterostructure of BT and doped BT. Although, BT is a classic ferroelectric material which has been intensively studied, new discoveries are yet to come when considering BT as one layer within oxide heterostructres [6]. Important differences between heterostructures such as BT on top of $SrTiO_3$ (STO) compared to BT and STO as single phase films have been observed for the first time by Tabata et al. [7]. In addition, Zhu Zhen-Ye et al. proved that the polarization of BT is much improved on a BT film deposited on STO than in the bulk form of BT [8]. In order to observe the PTCR effect in a heterostructure, it is essential that the layers are of high quality crystalline films. Polarisation direction must be easily controllable in order to observe the change in resistivity. One way of controlling the polarisation direction is by preparing epitaxial layers on top of one another. The same polarisation direction throughout the heterostructure may be achieved if heteroepitaxial films are deposited. This means that each deposited film should grow according to the structure of the underlying film. In the present work, thin films of pure and Nb-doped BT deposited by Pulsed Laser Deposition (PLD) on top of a thin film of $SrRuO_3$ (SRO - bottom electrode) on top of STO substrate are reported. The morphology, phase, thickness and the present ferroelectric domains are analysed with techniques such as XRD, SEM, AFM and PFM.

2. Experimental procedures

The PLD system used is a Tui Thin Film Star 248 nm KrF Excimer laser. Prior to deposition onto STO substrates, a number of experiments were carried out using Pt substrates in order to set the best deposition conditions. Therefore, the following parameters were set for the deposition process: a laser pulse frequency of 5 Hz, 200 mTorr O_2 partial pressure, a laser fluence of 2.3 Jcm^{-2} and a distance between the target and the substrate of 5 cm. The substrate temperature for the deposition of SRO was set at 675°C [9-11]. In addition, for the deposition of pure and doped BT, the substrate temperature was set at 600°C. The STO substrate was commercially bought (PI-KEM, UK), whilst the targets for the PLD process were prepared by a mixed-oxide route using raw powders. For the BT (pure and doped) targets, $BaCO_3$ (Sigma-Aldrich, 99.5%), TiO_2 (Sigma-Aldrich, 99.5%) and

Nb_2O_5 (Sigma-Aldrich, 99.5%), were mixed in stoichiometric quantities [5]. The powders were ball milled using zirconia balls as milling media, calcined at 1100°C and attrition milled. Subsequently, the powders were pressed into pellets and sintered at 1320°C in order to achieve a higher density. STO is a single crystal substrate with a cubic structure and (100) orientation. SRO - the first layer to be deposited also has a cubic structure with almost perfect match with STO (a mismatch of only +0.1254% with STO). The BT produced is expected to have a tetragonal structure. The mismatch between BT and STO is +2.2765% [12, 13]. Details on the crystallographic structure are shown in Table 1. In addition, the structure of the films is shown in Figure 1. Single crystal thin films are expected. Therefore, BT layer is expected to sit on the (001) plane, as shown in Figure 2. However, in order to maintain the unit cell volume, the (001) plane is expected to compress and therefore the c-axis to extend. The films are investigated using X-ray Diffraction (XRD) in order to identify the phase, structure and lattice parameters. The topography and the thickness are analysed using Scanning Electron Microscopy (SEM) and Atomic Force Microscopy (AFM). Piezoresponse Force Microscopy (PFM) is used to visualize the ferroelectric domains.

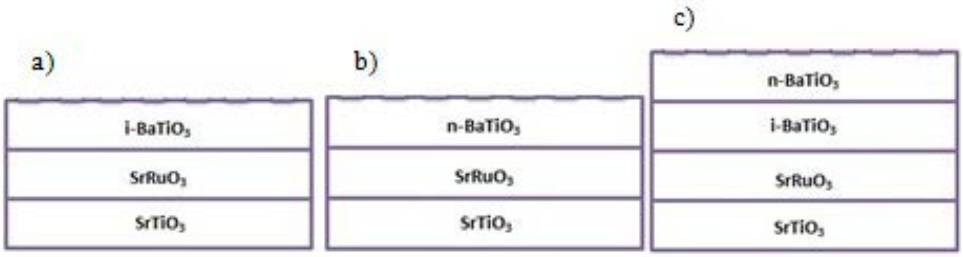

Fig. 1. The films deposited within this study: a) and b) are individual films of pure and Nb-doped deposited on SRO/STO for the purpose of investigations and c) represents the final heterostructure which consists of doped BT on top of pure BT on SRO/STO.

Table 1

Space group, lattice parameters and lattice mismatch with STO for the materials used [12,13]

Material	Space Group	Lattice Parameters Pseudocubic (Å)	Lattice Mismatch with $SrTiO_3$ (%)
$SrTiO_3$	Cubic Pm-3m (221)	a = b = c = 3.9051	
$SrRuO_3$	Cubic Pm-3m (221)	a = b = c = 3.91	+0.1254%
$BaTiO_3$	Tetragonal P4mm (99)	a = 3.9940 b = 3.9940 c = 4.0380	+2.2765%

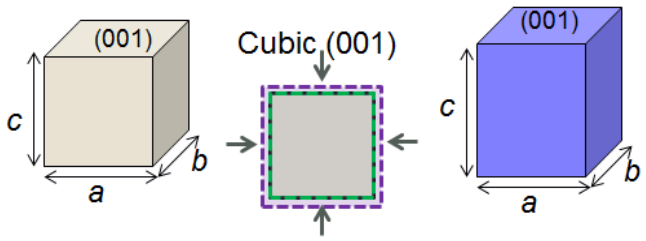

Fig. 2. Left – STO unit cell; right – BTO unit cell; centre – STO (grey), SRO (light green) and BT (violet) unit cells on top of each other; the figure highlights the match between STO and SRO and the mismatch with BTO.

3. Results and discussion

3.1 XRD

Diffractograms obtained from BT pellets, shown in Figure 3 a), indicate that a single phase polycrystalline ceramic has been prepared with a highly tetragonal crystal system, as expected. Figure 3 b) presents the XRD patterns obtained from the individual films deposited on SRO/STO, i.e. BT/SRO/STO, $BaNb_{0.01}Ti_{0.99}$/ SRO/STO and $BaNb_{0.02}Ti_{0.98}$/SRO/STO. It is noticed that the only peaks on the diffractograms, except the ones from the substrate, are (001) and (002) of BT, which indicates an epitaxial film. Figure 4 presents the rocking curves around the (001) peak, which have been carried out in order to check the degree of orientation of the single crystal films. BT peak didn't change its position in comparison to its position on the bulk ceramic diffractogram - Figure 3 a), which was expected assuming a change in the unit cell. It is concluded that the film is epitaxial, although the (001) did not change. In addition, the rocking curve on the film with 1% Nb dopant shows a Lorentz tail; however they are not as wide as seen in the rocking curve on the film with 2% dopant. This fact suggests that the film with more amount of dopant, i.e. 2% Nb, shows more strain and therefore a more disoriented structure. The full width at half maximum (FWHM) has been measured and the results are shown in Table 2. The FWHM provides information about the dislocation density in the film and/or strain in the structure. The values of FWHM obtained are 0.06^0 for the pure and for the doped BT layers, which compared to the value of 0.05^0 for the STO substrate (assumed to be instrumental broadening), suggest a perfect match between the epitaxial deposited films and the substrate. The small broadening is probably due to the instrument. One way to check whether the c-axis has extended is to work out the lattice parameters in BT powder and in BT epitaxial film on STO.

The lattice parameters for tetragonal BT powder are: a=3.9940 Å, b=3.9940 Å, c=4.0380 Å [14]. When depositing a material onto a single crystal substrate, an epitaxial film may be obtained if the materials possess matching lattice parameters. As BT sits on the (001) plane, a and b parameters are expected to be the same as for STO, i.e. a=b=3.9051 Å. In order to maintain a constant volume in the BTO unit cell, the c-axis is expected to increase from 4.0380 Å to 4.2239 Å. Therefore, the peak from the (100) plane of BT is expected to be seen at $\theta=10.5038^0$. This value was calculated using Bragg law: $n\lambda=2d\sin\theta$, where $\lambda=1.54$ Å is the wavelength of the X-rays emitted from a Copper tube.

However, the rocking curves of pure and doped BT films deposited on SRO/STO shown in Figure 4, show that the (001) peak didn't change its position compared to BT powder and therefore the c-axis of the unit cell didn't increase. One explanation to this behaviour may be given by a change in the unit cell volume. Another may be found in the details of the rocking curves. Although the curves suggest a highly oriented epitaxial film, their tails may contain more information. Therefore, further analysis is required. The software Fullprof has been used in order to fit the BT/SRO/STO rocking curve with two curves. The result is shown in Figure 5. Moreover, the FWHM values are shown in Table 3.

Comparing the FWHM from the fitted curves with the previous values, a massive difference is observed. The first fitted curve is a very narrow peak with a value of the FWHM of 0.05^0. However, the second peak is very broad with a value of the FWHM of 0.51^0. This suggests that the film has two regions with different orientations: the broad peak represents a less oriented interfacial region in the vicinity of the substrate, whilst the narrow peak represents a highly oriented region far from the substrate.

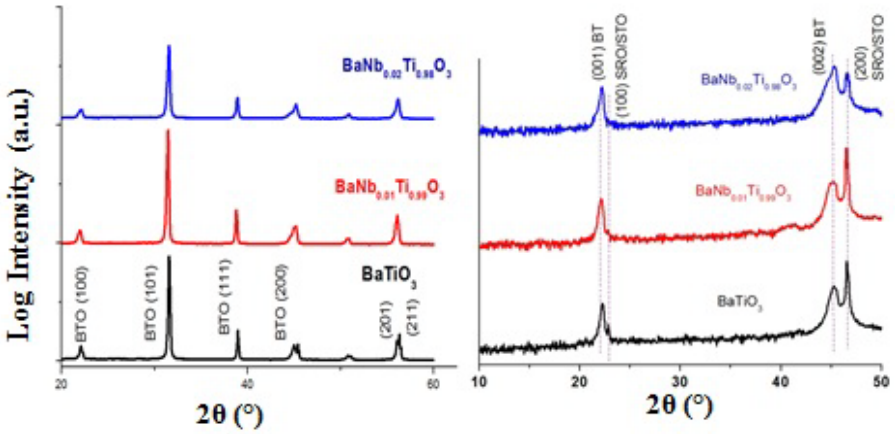

Fig. 3. a) Diffractograms of pure and doped BT sintered pellets; b) Diffractogram of pure and doped BT on SRO/STO substrate; on the figure, the peaks from the substrate as well as the peaks from the BT layer are labelled.

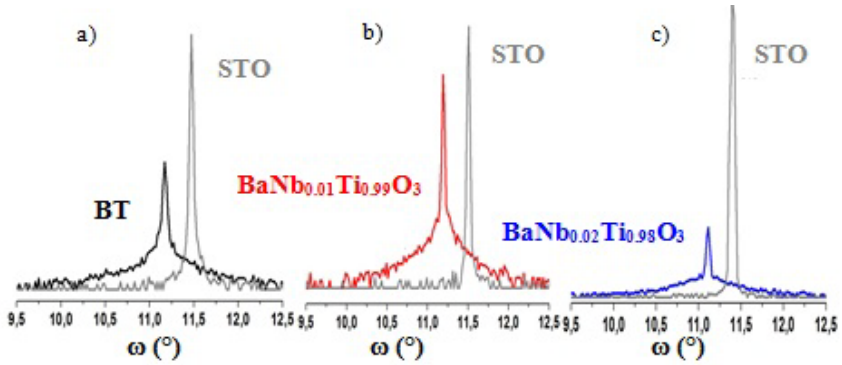

Fig. 4 Rocking curves of the individual films deposited onto SRO/STO: a) BT; b) $BaNb_{0.01}Ti_{0.99}$/ SRO/STO and c) $BaNb_{0.02}Ti_{0.98}$/SRO/STO compared with the rocking curve of the substrate STO

Table 2

FWHM values and their associated position according to the rocking curves on the pure and doped BT films deposited on SRO/STO substrates

Material	**Position (001) θ**	**FWHM (˚)**
$SrTiO_3$ substrate	11.39	0.05
$BaTiO_3$	11.13	0.06
$Ba(Ti_{0.99}Nb_{0.01})O_3$	11.14	0.06
$Ba(Ti_{0.98}Nb_{0.02})O_3$	11.14	0.06

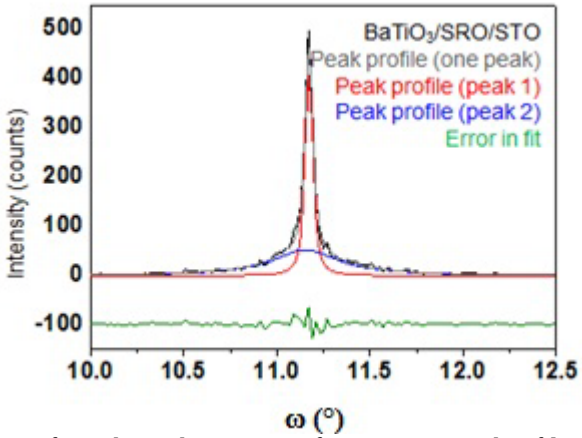

Fig.5. Two curve fit to the rocking curve of BT/SRO/STO thin film using Fullprof software.

Table 3

FWHM values for the fitted curves (BTO/SRO/STO film)

Material	**FWHM (˚)**
$BaTiO_3$	0.06
$BaTiO_3$ profile fit	0.06
Peak 1 (profile fit)	0.05
Peak 2 (profile fit)	0.51

The heterostructure has also been investigated with XRD and it has been noticed that the peaks from the STO substrate are very intense, therefore blocking the visualisation of the BT layers. Consequently, it has been decided to apply a 1° tilt angle to the sample. The obtained pattern is shown in Figure 6 a). A (001) orientation is indicated in both BT layers of the film. In addition, Figure 6 b) shows in more detail the diffractograms of the two heterostructures. It has been noticed that the sample with 2% Nb doping layer shows two separate peaks for BT, namely for the pure and for the doped BT. However, the sample with 1% Nb doping layer shows one single peak for BT which suggests a better lattice match between the BT and doped BT layers. Rocking curves obtained for the two heterostructures are shown in Figure 7. In addition, FWHM values have been calculated and they are presented in Table 4. It is clear that the FWHM values are higher in the heterostructures than the values for the films without a doped layer on top of BT. Therefore, there is more strain in the second deposited layer (BT) within the heterostructure, probably due to the top and bottom strain (from STO and doped BT layers). Moreover, when comparing the FWHM for the $BaNb_{0.01}Ti_{0.99}O_3$ and $BaNb_{0.02}Ti_{0.93}O_3$ peaks within the heterostructures, a higher value for 2% Nb-doped is observed. The unit cell parameters appear more strained in this case.

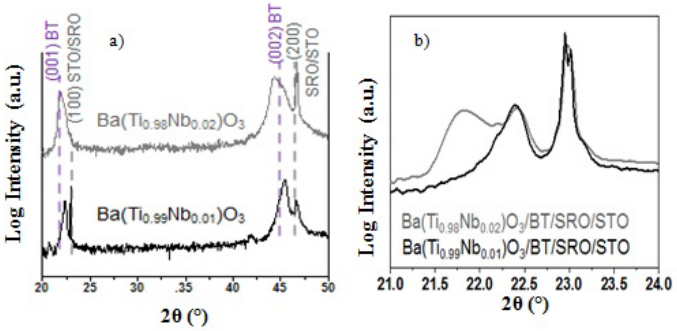

Fig. 6. a) Diffractograms of the two heterostructures with 1° tilt angle applied and b) Diffractogram of the heterostructures with no tilt in order to visualise the STO peak.

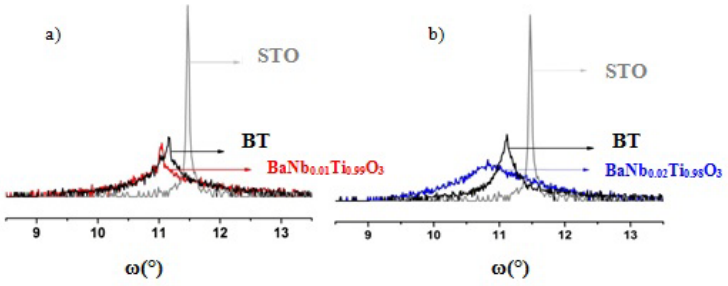

Fig. 7. Rocking curves for $BaNb_xTi_{(1-x)}O_3$/BTO/SRO/STO film for the three peaks: a) $BaNb_{0.01}Ti_{0.99}O_3$ and respectively b) $BaNb_{0.02}Ti_{0.98}O_3$, BT and STO.

Table 4

FWHM values for the rocking curves of the heterostructures

Material	**FWHM (˚)**
$BaTiO_3$ [$BaNb_{0.01}Ti_{0.99}O_3$/BTO/SRO/STO sample]	0.04
$BaNb_{0.01}Ti_{0.99}O_3$	0.25
$BaTiO_3$ [$BaNb_{0.01}Ti_{0.99}O_3$/BTO/SRO/STO sample]	0.26
$BaNb_{0.02}Ti_{0.98}O_3$	1.03

3.2 SEM

The heterostructure $BaNb_{0.02}Ti_{0.98}O_3$/BT/SRO/STO has been investigated with SEM. The cross section is shown in Figure 8 a). A film of approximately 150 nm thickness can be observed on the STO substrate. However, a distinction between the different layers of the film, i.e. $BaNb_{0.02}Ti_{0.98}O_3$/BT/SRO cannot be made. This is probably due to the good match between the crystal lattice parameters of these materials. Figure 8 b) shows the top surface of the film in discussion. The picture shows a very flat film with little surface topography. However, a few plate-like cubic structures can be observed. These are probably $BaNb_{0.02}TiO_3$ structures grown in the (100) direction – in agreement with the XRD patterns, where the (100) peak is the most intense.

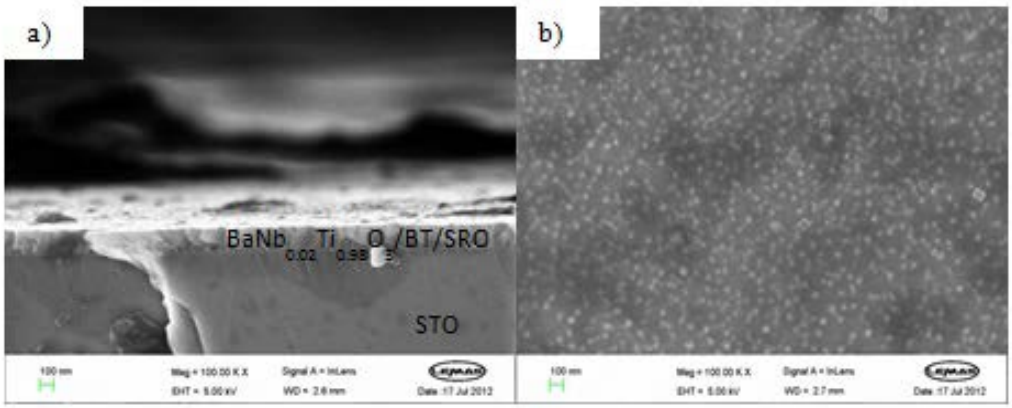

Fig. 8. a) Cross section of $BaNb_{0.02}Ti_{0.98}O_3$/BTO/SRO/STO thin film; b) Top surface of $BaNb_{0.02}Ti_{0.98}O_3$/BTO/SRO/STO thin film.

3.3 AFM

The topography of the heterostructure - $BaNb_{0.02}Ti_{0.98}O_3$/BTO/SRO/STO, was also analysed with AFM and the obtained image is shown in Figure 9 a). The surface looks relatively flat, with every change in peak-to-through distance observed in the profile - Figure 9 b), probably representing a grain. However, they are relatively small, with a size of approximately 0.1 μm. It may be inferred that

this structures are the plate-like cubic structures observed in SEM images. They do not look cubic, probably due to tip worn. The roughness of the film, measured as the maximum peak-to-trough, is approximately 4 nm, which represents a nearly smooth surface.

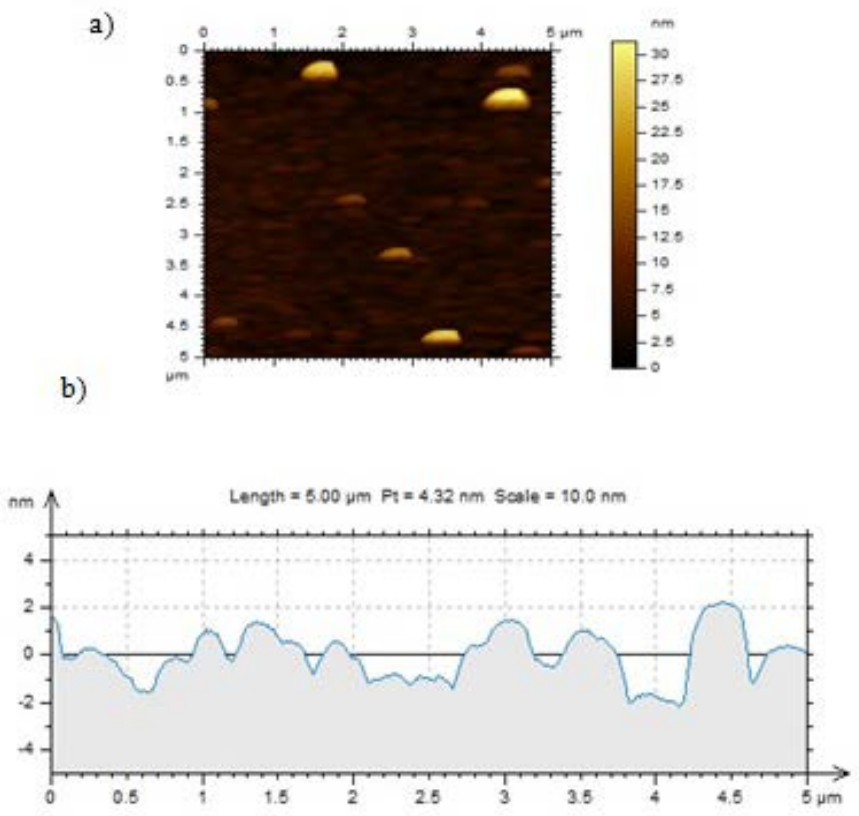

Fig. 9. Topography (a) and profile (b) of $BaNb_{0.02}Ti_{0.98}O_3$/BTO/SRO/STO thin film.

3.4 PFM

Fig. 10 a) (vertical phase) describes the polarization in the vertical direction. Hence, the darker brown regions indicate a polarisation pointing down. In contrast, the bright yellow regions show a polarisation pointing up. The contrast is relatively high, which indicates 180^0 out-of-phase domain structure. Furthermore, Fig. 10 b) depicts the magnitude of the piezoresponse related to the first figure. The contrast is lower; however it is lower for both polarisation directions which indicate a homogeneous material property.

The lateral phase is presented in Fig.10 c). Different domain polarity is observed, however there is much less order compared to vertical phase. The lateral amplitude is shown in Fig. 10 d). No signal can be visualised on this image, which indicates the low magnitude of any domains polarity existent in the lateral direction. It might be inferred that the signal detected in the lateral phase image is a result of the interference with the signal detected for the vertical phase component.

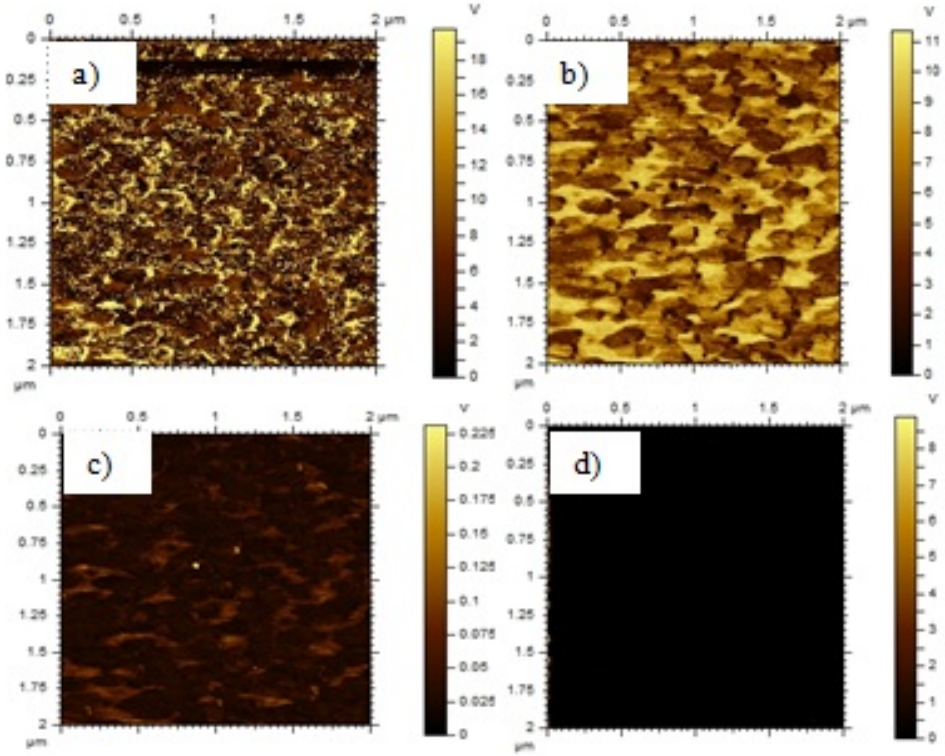

Fig. 10. PFM images of $BaNb_{0.02}Ti_{0.98}O_3$/BTO/SRO/STO thin film – a) phase vertical; b) amplitude vertical; c) phase lateral; d) amplitude lateral.

4. Conclusions

This work was designed to develop a novel mechanism for memory applications based on ferroelectric thin films. In summary, oxide heterostructures, namely: $BaNb_{0.02}Ti_{0.98}O_3$/BT/SRO/ STO and $BaNb_{0.01}Ti_{0.99}O_3$/BT/SRO/STO have been produced and high quality epitaxial films have been obtained, which are expected to show the PTCR effect at the interface.

Thin films were produced by PLD technique of which the optimum deposition conditions were investigated and obtained for both SRO (675°C) and BTO (600°C) layers. XRD, SEM, AFM and PFM were the characterisation

methods used to investigate the structural properties of each film deposited as individual layers as well as the heterostructures. The investigations proved a better lattice match between BTO and 1%-Nb doped BTO layer, when compared to BTO and 2%-Nb doped BTO layer. Therefore, the polarisation direction might be better controlled in the first sample, which is desirable for a controlled polarisation direction in order for the PTCR effect to occur. In addition, the surface of the heterostructures produced is relatively smooth with a surface maximum topography of 4 and, respectively, 5 nm, whilst the thickness of all layers deposited on STO substrate is of approximately 150 nm.

As future work, electrical measurements need to be made on the samples, such as current-voltage characteristics, polarisation-electric field hysteresis loops and leakage current measurements. This information is needed to understand the ferroelectric and transport properties of the films. Subsequently, investigations towards fabricating a device will be made.

R E F E R E N C E S

[1]. *V. Garcia and M. Bibes*, "Electronics: Inside story of ferroelectric memories", in Nature, **vol. 483**, no. 7389, 2012, pp. 279-281.

[2]. *J.F. Scott and C.A.P. De* Araujo, "Ferroelectric memories", in Science, **vol. 246**, no. 4936, 1989, pp. 1400-1405.

[3]. *S.V. Ducharme and A. Gruverman*, "Start the Presses", in Nature Materials, **vol. 8**, Jan. 2009, pp. 9-10.

[4]. *J.F. Scott*, Ferroelectric memories, Springer Verlag, Berlin, 2000.

[5]. *A. Moulson, J. Herbert*, Electroceramics, John Wiley & Sons Ltd, West Sussex, 1988.

[6]. *M. Stengel, D. Vanderbilt and N.A. Spaldin*, "Enhancement of ferroelectricity at metal–oxide interfaces", in Nature Materials, **vol. 8**, no. 5, 2009, pp. 392-397.

[7]. *H. Tabata, H. Tanaka and T. Kawai*, "Formation of artificial BaTiO3/SrTiO3 superlattices using pulsed laser deposition and their dielectric properties", in Applied physics letters, **vol. 65**, no. 15, 1994, pp. 1970-1972.

[8]. *Z. Zhen-Ye et al.*, "The first-principles study of ferroelectric behaviours of PbTiO3/SrTiO3 and BaTiO3/SrTiO3 superlattices", in Chinese Physics, **vol. 16**, no. 6, Jun 2007, pp. 1780-1786.

[9]. *K. Watanabe, M. Ami and M. Tanaka*, "Properties of polycrystalline SrRuO3 thin films on Si substrates", in Materials Research Bulletin, **vol. 32**, no. 1, 1997, pp. 83-96.

[10]. *M. Choi et al.*, "Structural and electrical properties of SrRuO3 thin films for buffer layers of coated conductors", in Physica C: Superconductivity, **vol. 463**, 2007, pp. 584-588.

[11]. *O. Gautreau et al.*, "Structural and electrical properties of room temperature pulsed laser deposited and post-annealed thin SrRuO3 films", in Thin solid films, **vol. 515**, no. 11, 2007, pp. 4580-4587.

[12]. *W. Bensch, H.W. Schmalle and A. Reller*, "Structure and thermochemical reactivity of CaRuO3 and SrRuO3", in Solid State Ionics, **vol. 43**, Mar. 1990, pp. 171-177.

[13]. H. E. *Swanson, R.K. Fuyat and G. M. Ugrinic, "Diffraction data"*, in National Bureau of Standards Circular, **vol. 539**, no. 3, 1954.
[14]. *M. Dawber, K. Rabe and J. Scott*, "Physics of thin-film ferroelectric oxides", in Reviews of modern physics, **vol. 77**, no. 4, Oct. 2005, pp. 1083-1130.